Local site symmetry and electronic structure of trialuminide and related intermetallic alloys probed by solid-state NMR

T. J. Bastow, C. T. Forwood, and M. A. Gibson
CSIRO Manufacturing Science and Technology, Private Bag 33, Clayton South MDC, Clayton, Victoria 3169, Australia

M. E. Smith
Department of Physics, University of Kent, Canterbury, Kent, United Kingdom
(Received 16 January 1998)

Intermetallic aluminide alloys with the $L1_2$, DO_{22}, DO_{23}, and Al_2Ti crystal structures have been examined by NMR using the ^{27}Al resonance to investigate how changes in crystal structure affect the local environment as indicated by hyperfine interactions at the atomic nucleus. All nonequivalent Al sites have been clearly resolved. Further, the environment of the transition metal component in each intermetallic crystal structure has been investigated using the ^{45}Sc resonance in the $L1_2$ structure of Al_3Sc, the ^{49}Ti resonance in the DO_{22} structure of Al_3Ti, and in Al_2Ti, the ^{51}V resonance in the DO_{22} structure of Al_3V and the ^{91}Zr resonance in the DO_{23} structure of Al_3Zr. Using a combination of static and magic-angle spinning Fourier transform NMR, and static field sweep spectroscopy, the isotropic Knight shifts (K_{iso}) and the nuclear quadrupole coupling constants (C_q) have been determined for all nuclei and all sites. In some cases the ^{27}Al axial Knight shift (K_{ax}) has been obtained. In the trialuminides each Al site located by NMR has been identified with the corresponding site in the unit cell of the crystal structure. [S0163-1829(98)05730-0]

INTRODUCTION

The aluminides are a group of alloys based on intermetallic compounds which have aluminium as a major component. They are currently of particular research interest as they have the potential for providing a new class of engineering materials capable of operating under hostile conditions at high temperature. The titanium aluminides are of particular significance as they possess combined properties of high elastic modulus to density ratio (E/s), and high yield stress with good creep and oxidation resistance at elevated temperatures, which makes them suitable candidates for use as light-weight materials in aerospace applications. Although considerable attention has been paid to alloys based on the titanium-rich $AlTi_3$ and equiatomic AlTi intermetallics,[1] it is the aluminium-rich trialuminide intermetallic Al_3Ti which exhibits the highest value of E/s ($\sim$57 GPa) and the best high-temperature oxidation resistance. However, with increasing aluminium content, the titanium aluminide intermetallics exhibit increased brittleness and it is the extreme lack of room temperature ductility that limits the practical application of alloys based on Al_3Ti. Attempts to overcome this problem have been made by the addition of transition metals as ternary alloying elements,[2–4] which transform the crystal structure of the binary Al_3Ti alloy from the brittle tetragonal DO_{22} structure to the potentially more ductile cubic $L1_2$ structure. Further, it has been demonstrated that an additional enhancement in ductility may be possible in $L1_2$ stabilized trialuminides if Ti-rich off-stoichiometric compositions are used. In this situation enhancement can occur via the activation of dislocation sources present at interfaces bounding intermetallic precipitates of Al_2Ti formed within the $L1_2$ matrix.[5] Similar stabilized $L1_2$ crystal structures have been fabricated by incorporating transition metal elements in the tetragonal DO_{23} crystal structure of the Al_3Zr intermetallic. Although these procedures have led to only modest improvements in ductility, it is clear that the development of practical alloys based on trialuminides will be critically dependent on gaining an understanding of how properties develop in association with changes in crystal structure from $L1_2 \rightarrow DO_{22} \rightarrow DO_{23} \rightarrow$the Al_2Ti crystal structure.

Figure 1 demonstrates that this series of crystal structures can be considered as a related sequence based on the $L1_2$ structure as a fundamental ''building block.'' The DO_{22} structure with $c/a \approx 2$ is formed when a repeating $L1_2$ structure is subjected to a shear $a/2[110]$ on consecutive (001) planes spaced at $a[001]$ apart. The DO_{23} structure with $c/a \approx 4$ is similarly formed from a repeating $L1_2$ structure, but in this case the $a/2[110]$ shears are on alternate (001) planes spaced $2a[001]$ apart. The Al_2Ti crystal structure with $c/a \approx 6$ is formed from a repeating $L1_2$ structure by the series of four nonconservative rigid body displacements indicated by the arrows.

NMR provides an atomic scale view of the structure of materials. ^{27}Al solid-state NMR is widely used[6] but has recently mainly concentrated on inorganic materials with relatively little work done on metallic compounds. In inorganic materials ^{27}Al exhibits an NMR chemical shift range of $\sim$100 ppm, but in metallic materials this is typically two orders of magnitude larger through the contact interaction with conduction electrons (termed the Knight shift K). NMR was applied vigorously to metals thirty years ago,[7] but is still not commonly used as a method of examining and characterizing conventional alloys and intermetallics. The main hindrance has been the extensive quadrupolar broadening that can result in loss of signal. NMR has developed considerably over the last two decades with much higher applied magnetic fields improving sensitivity, and more importantly

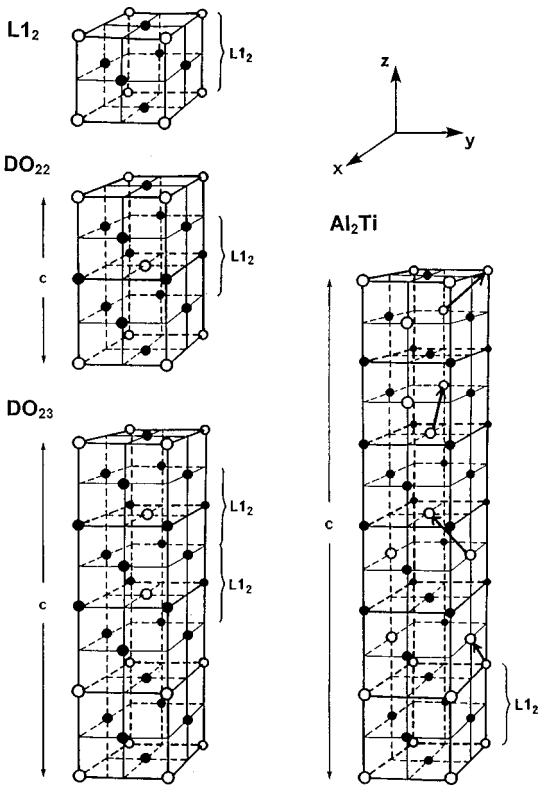

FIG. 1. Crystal structures for the aluminides discussed in this paper. ● ≡ Al; ○ ≡ transition metal.

reducing second-order quadrupolar effects. Magic-angle spinning (MAS) (Ref. 8) is commonly employed to improve resolution of NMR spectra by removing anisotropic interactions. Reports of MAS NMR from metallic specimens are extremely sparse.[8] Recently there have been a number of reports of ^{27}Al NMR (static and MAS) at high magnetic field, including $Mg_{17}Al_{12}$ and dilute alloys of aluminium in magnesium.[9] NMR of ^{27}Al has been reported from AlTi, $AlTi_3$ (Ref. 10), AlNi, and Al_3Ni_2 (Ref. 11) with C_q up to 16.37 MHz and Knight shift anisotropies (KSA's) of up to 130 ppm. MAS NMR of ^{27}Al has been reported from nanocrystalline Al_3Ti prepared by the reaction of organotitanium compounds with excess AlH_3 at 1000 °C, with the major peak appearing at 252 ppm, compared with 256 ppm for commercially prepared Al_3Ti.[12]

From an NMR spectroscopic point of view the large magnitude of the KSA leads to additional complications in analysis of the central transition $(\frac{1}{2}, -\frac{1}{2})$ line shape. For example, in AlTi and Al_3Ni_2 (Refs. 10 and 11) the perturbation this causes to the dominant quadrupole interaction is ~10–20 % and a relatively simple analysis separates the two contributions. However, for Al_2Ti and the trialuminides discussed below, the magnitude of the KSA is such as to perturb the central transition with an interaction at least comparable with, if not greater than the second-order quadrupolar interaction. This leads to a line shape which can be difficult to deconvolute unambiguously into separate sites with respective Knight shift, KSA (two or three parameters), and quadrupolar interaction (one or two parameters) for each site. The strategy adopted in the present work has been to evaluate the quadrupole interaction separately by locating the

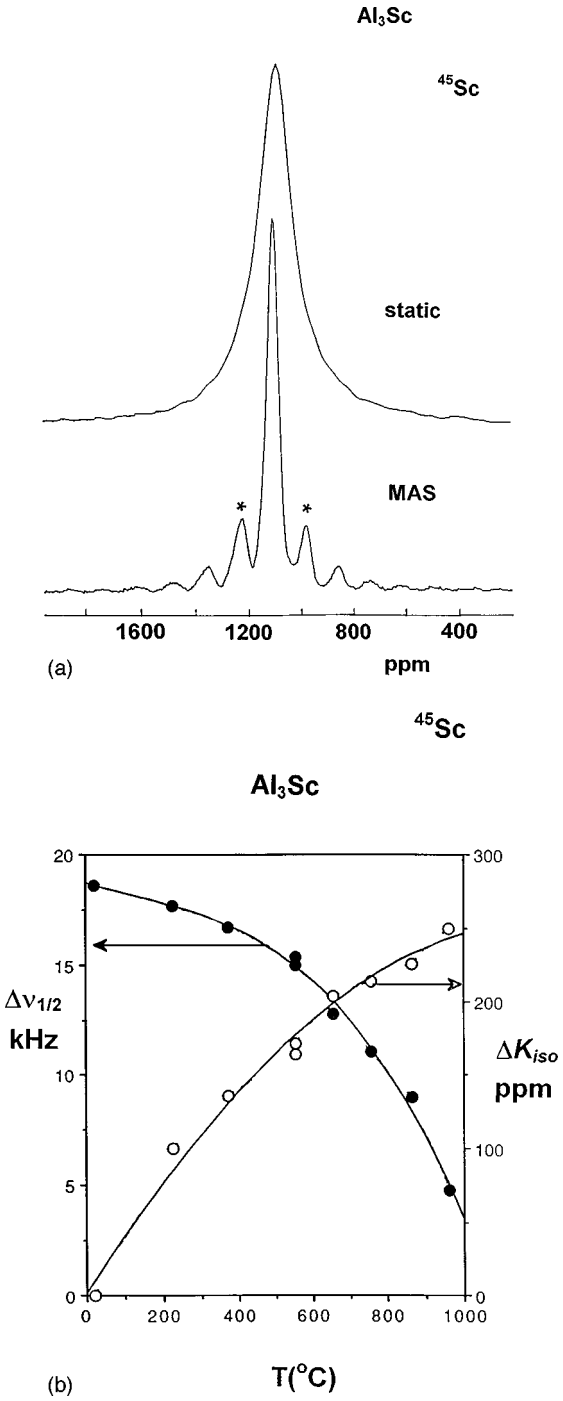

FIG. 2. Al_3Sc: (a) superposition of ^{45}Sc $(\frac{1}{2}, -\frac{1}{2})$ static and MAS spectra; (b) temperature dependence of the ^{45}Sc linewidth $\Delta\nu$ (FWHM) and Knight shift above its value at 295 K.

(much weaker) satellite transitions which are first-order quadrupolar broadened and hence are separated by integral multiples of $\nu_q = 3e^2qQ/2I(2I-1)h$. This approach was supplemented by using fast MAS (12–14 kHz) for the $(\frac{1}{2}, -\frac{1}{2})$ transition to determine accurately the individual Knight shifts in all five alloys, and to determine the quadrupolar interaction for each Al site for Al_2Ti where the satellite transitions were difficult to analyze. Furthermore the MAS spectra provided independent confirmation of the quadrupolar interaction evaluated from the satellite data for the trialuminides.

In this paper a series of intermetallic aluminide alloys with the $L1_2$, DO_{22}, DO_{23}, and Al_2Ti crystal structures are examined by NMR using the ^{27}Al resonance to investigate how changes in crystal structure affect the local environment (as indicated by local electric field gradients) at Al atomic sites, i.e., at the sites of the major atomic component of each intermetallic. In addition the environment of the transition metal component in each intermetallic crystal structure is investigated using the ^{45}Sc resonance in the $L1_2$ structure of Al_3Sc, the ^{49}Ti resonance in the DO_{22} structure of Al_3Ti, and in Al_2Ti, the ^{51}V resonance in the DO_{22} structure of Al_3V and the ^{91}Zr resonance in the DO_{23} structure of Al_3Zr. In the following the Al site nomenclature Al(1), Al(2), etc., is taken from the crystallographic data in Ref. 13.

EXPERIMENT

Sample preparation

Al_3Sc (with the $L1_2$ crystal structure), Al_3Ti and Al_3V (with the DO_{22} structure), Al_3Zr (with the DO_{23} structure), and Al_2Ti were prepared as 30 g ingots by argon-arc melting on a water cooled copper hearth using a nonconsumable tungsten electrode. Each ingot was homogenized by turning and melting five times with overall weight loss typically less than 0.01%. The ingots were heat treated at 1273 K for 1 week under argon at atmospheric pressure. After annealing, sections were cut from each ingot by spark machining and then mechanically polished and etched for examination by optical microscopy to confirm that they were essentially single phase. The remainder of each ingot was crushed and ground with a stainless steel pestle and mortar to produce a powder. The ferrous debris introduced during grinding was scrupulously removed with a small permanent magnet. The particle size was further reduced by sieving through a stainless steel mesh to produce a powder with a maximum particle dimension of ~ 50 μm. Each powder sample was reannealed under argon at 1273 K for 2 h to remove strains introduced by the grinding process.

NMR

Static ^{27}Al NMR spectra were obtained with a Bruker MSL 400 spectrometer using a superconducting magnet with a nominal field of 9.4 T, and operating at a frequency of 104.2 MHz. Frequency offsets of up to 2 MHz were used to observe the satellite transitions. For the room-temperature spectra a 4 mm MAS probe was used without sample rotation; purely for the convenience of the small coil and consequent small sample size, and the ability to accurately tune and match the probe. For work on Al_3Sc above room temperature a specially designed water-cooled probe was used, with a resistance furnace heating both specimen and coil, capable of operating continuously at temperatures up to at least 1233 K. The probe used a five turn transverse rf coil with an internal diameter of 7 mm. For these high-temperature measurements the samples were sealed under vacuum in quartz capsules.

To observe the broad lines in these alloys, all spectra were obtained using an echo sequence, $D1\text{-}t\text{-}D2\text{-}t\text{-}acq$, with phase cycling which efficiently cancelled any transmitter pulse breakthrough.[14] To ensure a uniform power spectrum

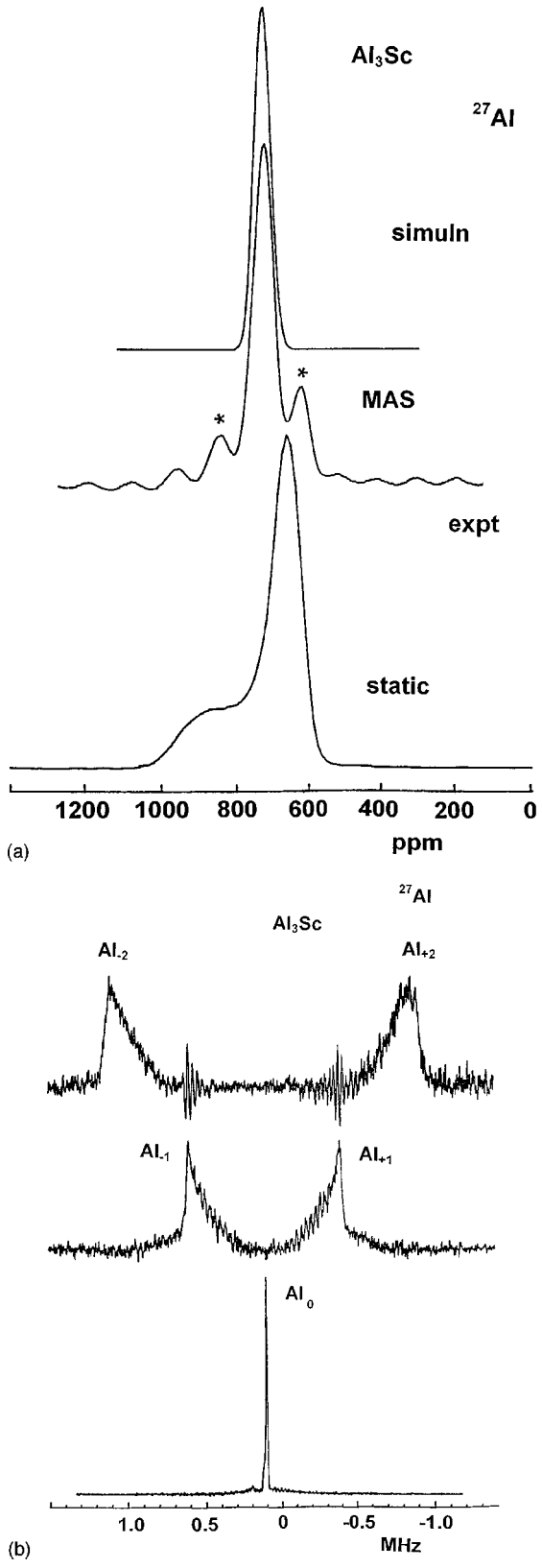

FIG. 3. Al_3Sc: (a) superposition of ^{27}Al $(\frac{1}{2}, -\frac{1}{2})$ static spectrum (below), MAS spectrum and MAS simulation (above); (b) superposition of static $(\frac{1}{2}, -\frac{1}{2})$, and $\pm(\frac{1}{2}, \frac{3}{2})$ and $\pm(\frac{3}{2}, \frac{5}{2})$ satellite line shapes. [Note satellite labelling in the figures, e.g., $Al(2)_{-1} \equiv Al(2)$ site $(-\frac{1}{2}, -\frac{3}{2})$ transition].

TABLE I. Structures and NMR data for transition metal aluminides.

Material	Structure	Space Group	Type	Nucleus	C_q (MHz)	η	K_{iso} (ppm)[a] K_{ax}
Al_3Sc	Cubic	$Pm3m$	$L1_2$	^{45}Sc	0	0	1100
				^{27}Al	6.80	0	756; $K_{ax}\approx 40$
Al_3Ti	Tetragonal	$I4/mmm$	DO_{22}	^{49}Ti[d]	15.5	0	2750
				^{27}Al Al(1)	11.37	0	335
					(11.20)[b]		
				^{27}Al Al(2)	3.30	0	253
Al_2Ti	Tetragonal	$I4_1/amd$	$GaHf_2$	^{49}Ti[d]	8.5	0.7	3300
				^{27}Al Al(1)	6.0	0.9	330
				^{27}Al Al(2)	9.2	0.47	610
AlTi	Tetragonal	$P4/mmm$	$L1_0$	^{49}Ti[d]	13.8	0	5000; $K_{ax}=260$
				^{27}Al[c]	8.15	0	-170; $K_{ax}=130$
$AlTi_3$	Hexagonal	$P6_3/mmc$	DO_{19}	^{49}Ti[d]	13.9	0.1	3600
				^{27}Al[c]	≈ 0		200; $K_{ax}=270$
Al_3V	Tetragonal	$I4/mmm$	DO_{22}	^{51}V	6.13	0	185; $K_{ax}\approx 100$
				^{27}Al Al(1)	2.50	0	-97
				^{27}Al Al(2)	11.39	0	-130
Al_3Zr	Tetragonal	$I4/mmm$	DO_{23}	^{91}Zr	7.33	0	40; $K_{ax}\approx 0$
				^{27}Al Al(1)	9.05	0.03	455
				^{27}Al Al(2)	3.84	0	384
				^{27}Al Al(3)	11.33	0	687
					(11.45)[b]		

[a]Shift zero: ^{27}Al:$Al(H_2O)_6^{3+}$; ^{49}Ti:$SrTiO_3$, ^{51}V:$NaVO_3$ (meta), ^{91}Zr, $BaZrO_3$, ^{45}Sc:$ScCl_3(aq)$.
[b]Value obtained from MAS.
[c]Data from Ref. 10.
[d]Data from Ref. 18.

over the ^{27}Al lines encountered here, sub-90° rf pulses $D1 = D2 = 2$ μs were used with an echo time of 20 μs. The ^{27}Al spectra were referenced to ^{27}Al in $Al(H_2O)_6^{3+}$ at zero ppm shift, via the ^{27}Al resonance from octahedrally coordinated aluminium in $Y_3Al_5O_{12}$ at 0.7 ppm. The NMR reference frequencies for the transition metals, set at 0 ppm in each case, were obtained from the following compounds: $ScCl_3$ (aq), $SrTiO_3$, $NaVO_3$ (meta), and $BaZrO_3$. The frequency axes for the spectra displayed here are graduated in either ppm (parts per million) or kHz shift from zero. Some additional static spectra of the central transition were accumulated at magnetic fields of 7.05 and 14.1 T using the same techniques as at 9.4 T.

Static spectra of the satellites were recorded either piecewise by ≈500 kHz sections using Fourier transform (FT) NMR (at 9.4 T) or by field sweeping (using echoes) over the whole range (at 7.05 T). The limiting sweep width of ≈500 kHz for the FT NMR traces was set by a combination of the inverse of the 2 μs pulse lengths used for the echo formation and the bandwidth of the probe. The latter was increased from its unloaded value to close to 500 kHz by the detuning effect of the metallic specimen. The field sweep at 7.05 T was carried out on a Chemagnetics CMX-300 spectrometer where the superconducting magnet is equipped with an additional superconducting sweep coil capable of providing ±0.5 T. The main field is controlled by varying the current in the sweep coil directly from the pulse program. At each field setting a spin echo is accumulated using ''soft'' 45 μs 90° pulses. At 9.4 T MAS at 10–12 kHz rotation frequency was applied. For the MAS runs, to reduce the rotational drag due to induced eddy currents, the alloy specimen was diluted with MgO powder. In the MAS spectra shown below the spinning sidebands are denoted by an asterisk.

RESULTS

Al_3Sc

This compound is cubic with the $L1_2$ structure. The Sc site has cubic point symmetry $m3m$ which ensures that both the electric field gradient and quadrupole asymmetry parameter (η) will be zero. The cubic site symmetry is reflected in the symmetric ^{45}Sc resonance that is relatively narrow [Fig. 2(a)] unlike ^{45}Sc in most noncubic compounds where significant quadrupolar interaction occurs. MAS at 11.7 kHz narrows the line symmetrically by a factor of approximately 3. Note that in pure metallic aluminium (fcc) the static linewidth decreases by over an order of magnitude by MAS at 12 kHz. The ^{45}Sc static line in Al_3Sc is broadened by dipole-dipole interaction and Knight shift dispersion due to the presence of atomic defects. The latter contribution will not narrow with MAS. Calculation of the dipole-dipole second moment at the Sc site yields a linewidth (assuming a Gaussian line shape) of 8.6 kHz, whereas the observed full width at half maximum (FWHM) is 15.7 kHz. The discrepancy can be attributed to Knight shift dispersion. Comparison of static linewidths at 9.4 and 14.1 T show a larger linewidth at the higher field, consistent with a Knight shift dispersion contribution which will increase linearly with field.

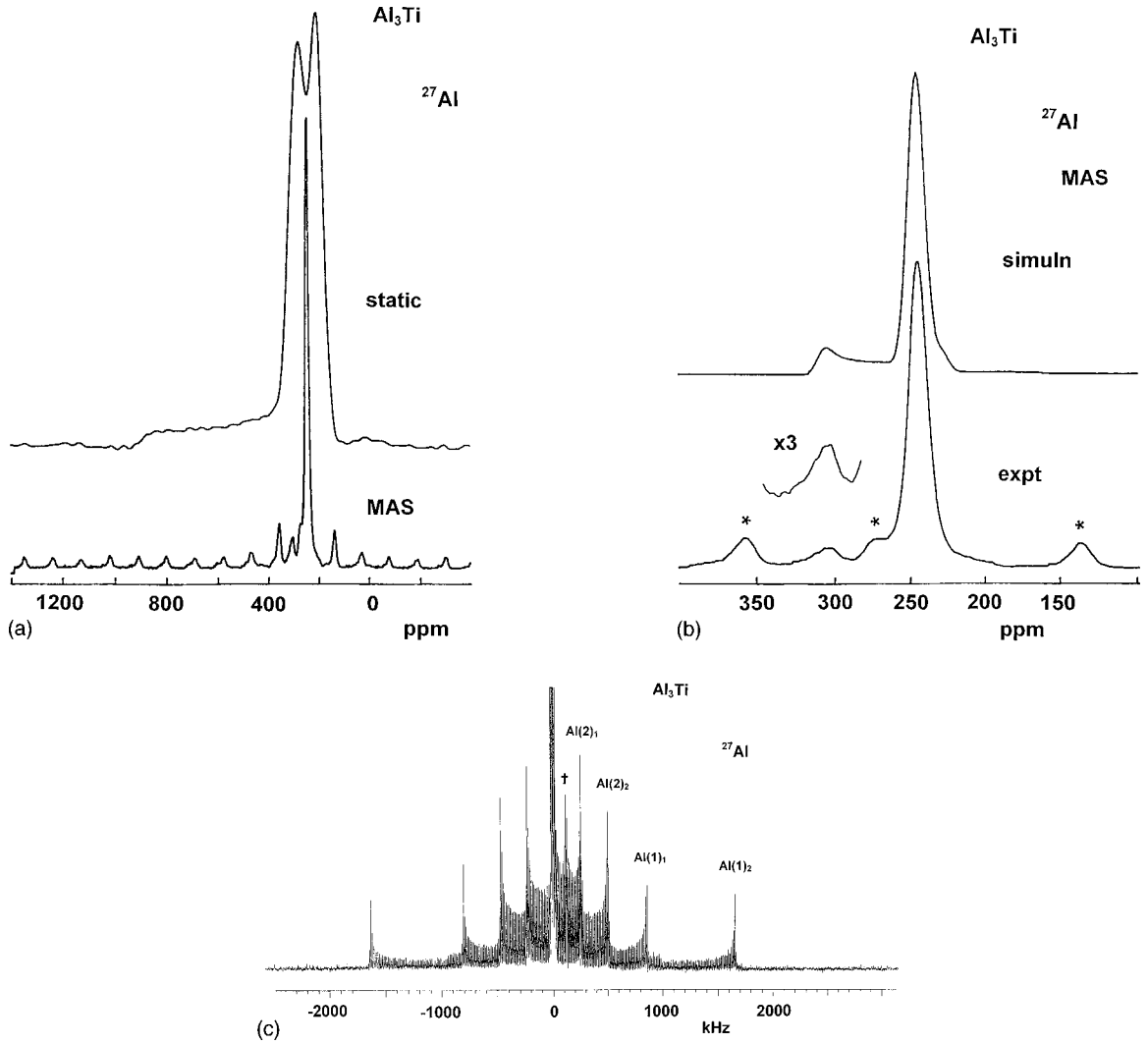

FIG. 4. Al_3Ti: (a) superposition of ^{27}Al $(\frac{1}{2}, -\frac{1}{2})$ static and MAS; (b) expansion of the MAS spectrum in (a) (below) and simulation (above); (c) ^{27}Al static field sweep of $\pm(\frac{1}{2}, \frac{3}{2})$ and $\pm(\frac{3}{2}, \frac{5}{2})$ satellite line shapes. [Note that metallic Al in the specimen gives rise to the spinning sideband (*) immediately to the left of the central transition in (b) and the line marked with dagger at 128 kHz in (c)].

The temperature variation of both the linewidth $\Delta\nu$ and Knight shift is shown from room temperature to 1233 K in Fig. 2(b). There is a strong Knight shift dependence on temperature which has also been observed for ^{67}Zn in zinc metal[15] and ^{111}Cd in cadmium metal[16] where it was attributed to the averaging out of the lattice anisotropy by the lattice vibrations and the consequent increase in the *s* character of the electronic wave function at the metal atom site. The ^{45}Sc linewidth change with temperature is such that the temperature at which the ^{45}Sc linewidth is $\frac{1}{4}$ of the low T (rigid lattice) limit corresponds to about $0.78T_m$ (where T_m is the melting point). For Al_3Sc therefore the observations are in accord with line narrowing caused by the onset of atomic (Sc) diffusion. For Al_3Sc an analysis for activation energy for hopping of ^{45}Sc comparable to that made for ^{27}Al in aluminium metal where the corresponding temperature is approximately $0.68T_m$ (Ref. 17) cannot be accurately done since linewidth measurements at sufficiently high temperatures were not possible with the present furnace. In the present context it might be noted that in the case of $Ni_{1-x}Al_x$, with $x>0.52$, ^{27}Al linewidth measurements indicate that the constitutional vacancies associated with the nonstoichiometry assist Al diffusion at anomalously low temperatures relative to the melting point.[11]

In the $L1_2$ crystal structure of Al_3Sc there is a single Al site with $4/mmm$ point symmetry which is axially symmetric. The $(\frac{1}{2}, -\frac{1}{2})$ line shape [Fig. 3(a)], with the pedestal on the low frequency side, is interpreted as due principally to KSA, since the MAS line lies close to its centroid. This interpretation is reinforced as the frequency width of the line varies proportionately with the applied magnetic field. A direct measurement of the static line shape yields $K_{ax} = K_{33} - K_{11} = 340$ ppm. This is only an approximate result since there must in principle be a quadrupole interaction, but for the $(\frac{1}{2}, -\frac{1}{2})$ lineshape, neither static nor MAS (at 11.7 kHz) give an indication of any quadrupolar interaction. A systematic search yields the powder line shapes of the four first-order quadrupolar satellites [Fig. 3(b)]. From the satellite spacing the C_q for ^{27}Al can be derived (Table I).

Al_3Ti

The structure here is tetragonal, with a fourfold axis at the Ti and the two nonequivalent Al sites which guarantees elec-

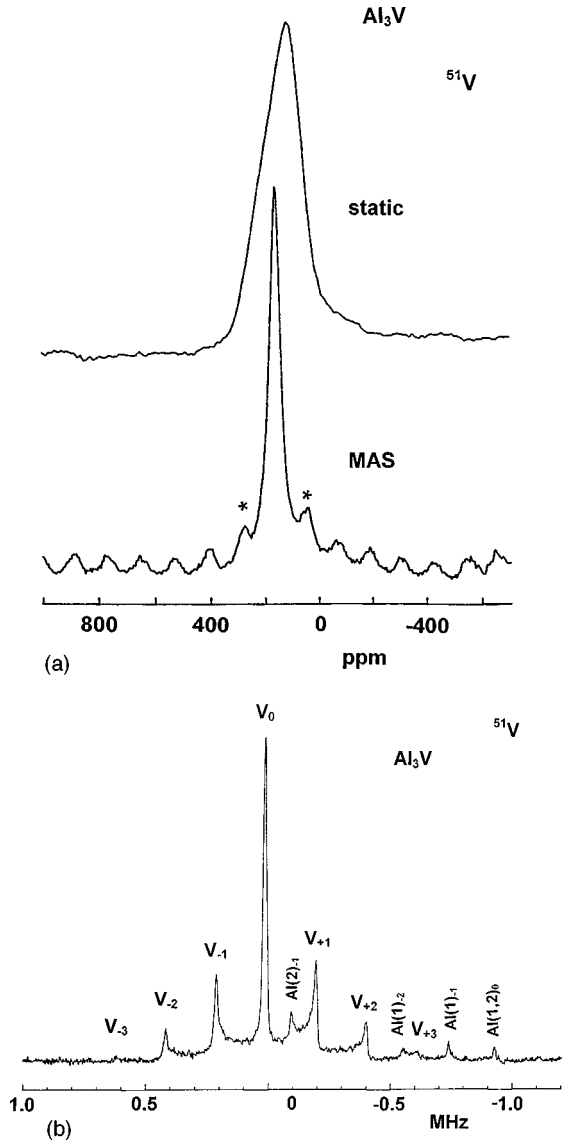

FIG. 5. Al_3V: (a) superposition of ^{51}V $(\frac{1}{2}, -\frac{1}{2})$ static and MAS spectra; (b) central transition plus the inner satellites.

tric field gradients with $\eta=0$ in each case. The nuclear hyperfine details for $^{47,49}Ti$ are reproduced in Table I from a separate report of titanium NMR from such alloys.[18] Titanium (^{49}Ti) experiences a significant quadrupolar interaction of 15.5 MHz which is largely a result of its moderate quadrupole moment.

There are two nonequivalent Al sites in the unit cell, populated in the ratio 1:2 (see Fig. 1). The designated Al(1) in position $2b$ with point symmetry $4/mmm$ which lies in planes containing Ti and Al atoms parallel to (001), and the site Al(2) in position $4d$ with point symmetry $4m2$ which lie in alternate planes and contain only Al atoms. The $(\frac{1}{2}, -\frac{1}{2})$ line shape, with an extended high frequency pedestal [Fig. 4(a)], indicates a major contribution from KSA. Simulation of this line shape [Fig. 4(b)] to give K_{iso}, KSA, and C_q components for the two sites was ambiguous since eight parameters are required for each site. However, by varying the applied magnetic field it was clear that the central transition lineshapes had contributions from both KSA and second-order quadrupolar effects. In fact using the quadrupolar interaction calculated from the satellite transition (*vide infra*) gives a second-order quadrupolar width of 39 kHz at 9.4 T compared to the 24 kHz measured. The first-order quadrupolar satellites were observed by conventional FT NMR at 9.4 T (not shown here) and by field sweep at 7.05 T [Fig. 4(c)]. On the basis of the line shape intensities in the field sweep spectrum, the site with the smaller C_q can be assigned to Al(2). The aluminum sites both rigorously have $\eta=0$, but with significantly different C_q. MAS was able to locate the individual K_{iso}, with MAS at 11.5 kHz being able to fully narrow the resonance from the site with the smaller C_q. Simulation of the centreband can be correlated to the features observed in the MAS spectrum, with the larger C_q site underlying the narrow resonance. The high frequency singularity is clearly resolved in Fig. 4(b), whereas the lower frequency singularity appears under the narrow line. Simulation of these lines, using the quadrupole coupling constants obtained from the first-order satellites, yields the Knight shifts (Table I). Note that the presence of a resonance from metallic aluminum in Figs. 4(b) and 4(c) suggests that the overall composition of the alloy was slightly on the aluminum-rich side of the Al_3Ti line compound.

Al_3V

This compound is isostructural with Al_3Ti. The single V and two Al sites have $\eta=0$. The ^{51}V central transition is relatively featureless in Fig. 5(a), apart from a small step on the low frequency side. Interpreting this feature as due to KSA's leads to an estimate of K_{ax} of approximately 100 ppm ($\approx$10 kHz). The static linewidth of the central transition scales proportionally with the applied magnetic field confirming KSA as the dominant broadening mechanism. MAS yields line narrowing by a factor of approximately 4. The observed static line shape would conceal the calculated second-order quadrupolar linewidth obtained from the satellite data (below) of 4.8 kHz. With the addition of a dipolar or disorder broadening factor, the line shape can be simulated, with the C_q value derived from the satellite data, to yield the isotropic Knight shift. Since the magnetic moment of ^{51}V is very close to that for ^{27}Al, the satellite structures for the two nuclei overlap. A detailed spectrum is observed [Fig. 5(b)] with three pairs of satellites, viz. $\pm(\frac{1}{2}, \frac{3}{2})$, $\pm(\frac{3}{2}, \frac{5}{2})$, and $\pm(\frac{5}{2}, \frac{7}{2})$ clearly resolved, and interlaced with the ^{27}Al satellites. A C_q value for ^{51}V was derived from the satellite spacings and is listed in Table I.

The ^{27}Al central transition static line shape in Fig. 6(a) suggests possible KSA contributions, but decomposition into two component line shapes is somewhat ambiguous. The MAS line shape, however, can be easily resolved, as for Al_3Ti, into a fully narrowed line from the low C_q site and a second-order quadrupolar line shape from the high C_q site. The simulation in Fig. 6(b), performed with the C_q values derived from the satellite data [shown in part in Fig. 6(c)], yielded the Knight shifts (see Table I). From the C_q derived from the satellite data the second-order quadrupolar width can be calculated and at 7.05 T there is good agreement between calculated and measured linewidths. However, on increasing the applied magnetic field the linewidth is significantly greater than expected from quadrupolar broadening

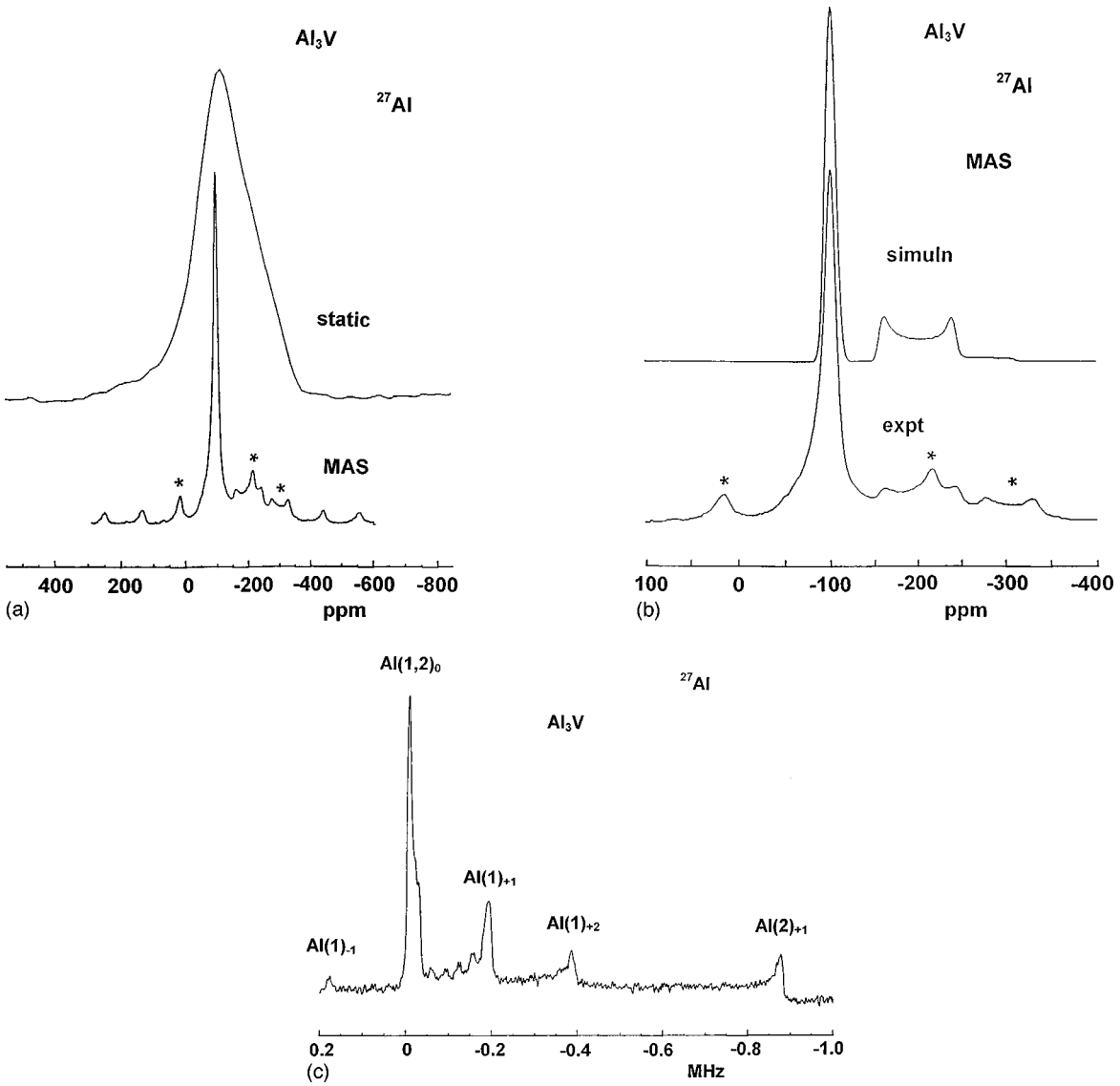

FIG. 6. Al_3V: (a) superposition of ^{27}Al $(\frac{1}{2}, -\frac{1}{2})$ static and MAS spectra and MAS simulation; (b) expansion of MAS spectrum and simulation; (c) central transition plus inner high frequency satellites.

alone, thus indicating that KSA is making an increasingly important contribution to the line shape.

Al_3Zr

The crystal structure for Al_3Zr is body-centered tetragonal with a fourfold axis at the Zr and at two of the three nonequivalent Al sites, which guarantees $\eta=0$ in each case. At the third Al site the point symmetry is only *mmm* which allows $\eta>0$.

The static ^{91}Zr NMR spectrum of the central transition in Fig. 7 can be analyzed to give $C_q=7.3$ MHz, assuming that the line shape is due solely to second-order quadrupolar interaction, and as expected for a site with fourfold axial symmetry this gives rise to an $\eta=0$ pattern. This value for C_q may be compared to the value for hcp zirconium metal of $C_q=18.2$ MHz at 296 K, and moreover, the Knight shift of 40 ppm is interestingly close to zero compared to that for zirconium metal of 3500 ppm.[19] It is likely that for Al_3Zr the positive *s*-contact and *d*-orbital terms are fortuitously nearly cancelled by the negative *d*-core polarization term.

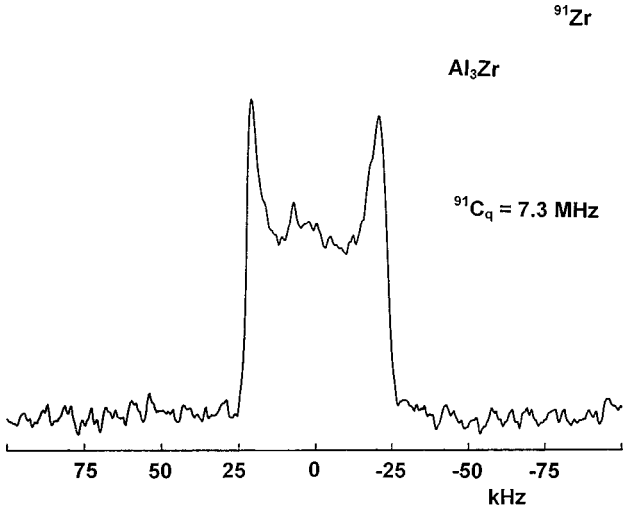

FIG. 7. Al_3Zr: ^{91}Zr $(\frac{1}{2}, -\frac{1}{2})$ static line shape.

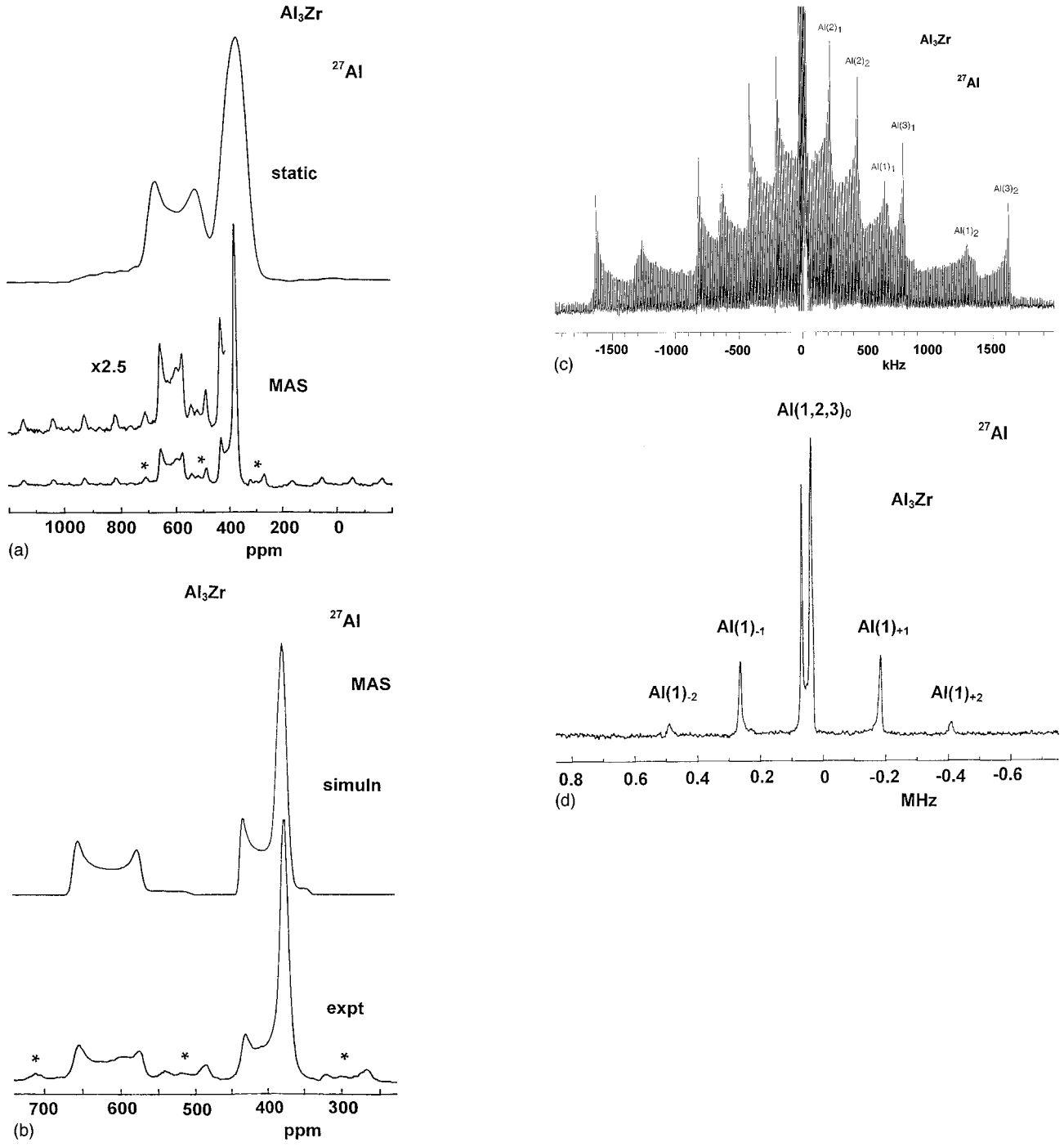

FIG. 8. Al_3Zr: (a) superposition of ^{27}Al $(\frac{1}{2}, -\frac{1}{2})$ static and MAS spectra; (b) expansion of MAS spectrum (below) and simulation (above); (c) field sweep of satellites; (d) FT NMR spectrum of inner satellites.

Inspection of the ^{27}Al central transition static line shape in Fig. 8(a) suggests a possible contribution of a second-order quadrupolar line shape from one of the Al sites. There is most probably a large contribution from KSA making analysis using second-order quadrupolar broadening alone ambiguous, and it is unclear how the static spectrum should be deconvoluted. However MAS provides a clear separation into three contributions: a narrow line and two second-order quadrupolar lines which can be simulated with the values obtained from the satellite data in Figs. 8(c) and 8(d), giving the Knight shifts (Table I).

The C_q for the three nonequivalent Al sites can be determined directly from the satellite spectrum of Fig. 8(c). The powder line shape for the $\eta > 0$ site, Al(1) has a peak at $(1-\eta)\nu_q$ and an edge at $(1+\eta)\nu_q$ for the $\pm(\frac{1}{2}, \frac{3}{2})$ transition, and at twice these values for the $\pm(\frac{3}{2}, \frac{5}{2})$ transition. These features can be identified for a set of four of the observed satellite peaks in both field sweep data and the FT NMR data (not shown). This identifies the Al(1) site. The C_q values for the two axially symmetric line shapes were assigned to specific crystallographic sites in the DO_{23} structure by assuming that the $4m2$ site, in DO_{22} Al_3Ti, had split, in DO_{23} Al_3Zr, into the nonaxial mmm site [Al(1)] and another (low C_q) $4m2$ site [Al(2)], and that the $4/mmm$ site, in Al_3Ti, had translated into the (high C_q) $4mm$ site [Al(3)] in Al_3Zr. The

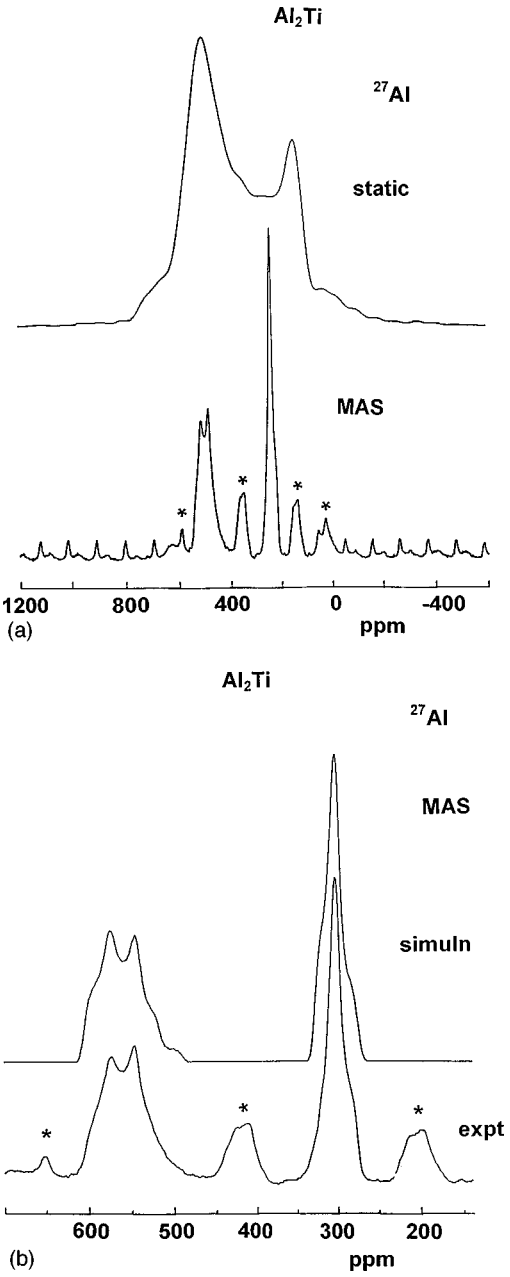

FIG. 9. Al_2Ti: (a) superposition of ^{27}Al ($\frac{1}{2}$, $-\frac{1}{2}$) static and MAS spectra; (b) expansion of MAS spectrum (below) with simulation (above).

allocated coupling constants, and a value of η for Al(1) are given in Table I.

Al_2Ti

The Al_2Ti intermetallic has a crystal structure, based on the $HfGa_2$ structure, with one Ti site and two nonequivalent Al sites (Fig. 1) which represents a further, even more elaborate stacking variant of the basic $L1_2$ unit. Particular care was taken to confirm the structure and purity of the phase for this specimen using x-ray diffraction (XRD). Excellent simulation of the observed XRD pattern structure was obtained using the published a and c parameters for Al_2Ti and the z parameters for Hf and Ga(1) and Ga(2). The point symmetry of the Ti, Al(1), and Al(2) sites is $2mm$, so there is a finite asymmetry parameter at each site. The nuclear hyperfine details are reproduced in Table I from a separate report.[18]

The observed static ^{27}Al line shape of the central transition in Fig. 9(a) is not obviously decomposed into two $\eta > 0$ line shapes and indicates a considerable KSA component at each site. However, once again the MAS spectrum clarifies the situation, exhibiting two high η sites from which a powder simulation [Fig. 9(b)] yields C_q, η, and K for each site. They have been assigned arbitrarily since it is not clear which set of nuclear parameters belongs to which of the two distinct crystal sites that have identical point symmetries. Satellite spectra were obtained but proved difficult to analyze and are not shown here since the MAS spectrum of the ($\frac{1}{2}$, $-\frac{1}{2}$) transition gave the nuclear hyperfine interaction parameters data unambiguously.

DISCUSSION

The considerable amount of multinuclear magnetic resonance data obtained here shows the very detailed structural information that can be extracted from such an approach for all the sites in the different structures. The ^{45}Sc, ^{51}V, ^{91}Zr, and ^{49}Ti (in Al_3Ti and Al_2Ti) all accurately confirm the diffraction-determined site multiplicity. Small deviations from axial symmetry in these systems are readily detected in the satellite powder spectrum [e.g., Al(1) in Al_3Zr] whereas the lower site symmetries for Ti and Al in Al_2Ti were reflected in the high η values obtained from the analysis of the central transition line shapes. In these materials the ^{27}Al NMR spectra show mixed C_q/KSA interactions which are more difficult to analyze than in insulating materials where chemical shift anisotropy is usually negligible. Detailed unambiguous deconvolution is difficult but by combining static observation of the central and satellite transitions, as well as examining the central transition with MAS, estimates of the interactions can be readily made. The ^{27}Al NMR data shows a wide variation in K, C_q, and η as the crystal structure changes, with the most obvious being the number and intensity of the resonances reflecting the multiplicity of the sites. In the $L1_2$ and DO_{22} structures the resonances all have $\eta = 0$ as expected, but with significantly different C_q. That this is a consequence of the structure rather than the other element is well illustrated by how similar the C_q are between Al_3Ti and Al_3V. However, in contrast, K is a very sensitive function of the second element as expected since it will contribute differently to the electron band structure. The K_{iso} range for ^{27}Al observed here is from 756−−130 ppm. Detailed rationalization of the C_q and K_{iso} values is not merited without theoretical calculation of the separate band structures. Such *ab initio* methods have recently successfully reproduced the C_q values for the elemental hexagonal metals.[20]

It should be noted here that a previous report on nanocrystalline Al_3Ti (Ref. 12) gave the ^{27}Al shift as 252 ppm. The work reported here indicates that this signal comes from only one of the Al sites (the smaller C_q) but there is no evidence in Ref. 12 of the other site which, even under MAS, is broad and could be lost if there is sufficient local strain or other perturbation at the Al sites. Examples demonstrating such an effect were encountered during the course of this work for two alloys with the $L1_2$ structure, viz. $AlNi_3$ and $Al_{67}Cr_9Ti_{24}$, for which the ^{27}Al spectra were examined. In

each case the ^{27}Al line was broad and structured, with linewidths of order 120 kHz. In the case of $AlNi_3$, the ^{27}Al resonance linewidth may be compared with that of ^{45}Sc in Al_3Sc (15.7 kHz); the much greater linewidth observed in $AlNi_3$ may be due to magnetic fluctuations at Al sites due to the Ni ions. In the case of $Al_{67}Cr_9Ti_{24}$ the ^{27}Al resonance linewidth should be compared with that of ^{27}Al in Al_3Sc (major feature, 10 kHz). Here the random substitution of Cr for Al (Ref. 21) will presumably lead to deviations of the local symmetry at the Al sites from 4/*mmm*, and thus a spectrum of electric field gradients yielding the observed line broadening.

CONCLUSION

Comprehensive multinuclear NMR data from a series of trialuminide and related intermetallics provides detailed atomic scale site information. The spectra from which this information was extracted were obtained by a combination of conventional FT NMR (both static and MAS) at different fields, and field sweep acquisition at 7.05 T. Such a combination was necessary to properly disentangle the different contributions to the nuclear Hamiltonian. Precise nuclear hyperfine data has been obtained which should provide constraints and checks for a band structure based calculation of C_q and (eventually) $K_{\rm iso}$. The Al site symmetry and multiplicity in these alloys determined by NMR neatly confirms the information previously provided by x-ray crystallography. Such an approach can be used to probe changes in these alloys with composition and processing. It can be anticipated that solid-state NMR will be increasingly used to probe such materials.

ACKNOWLEDGMENTS

The authors thank D. G. Hay for the x-ray confirmation of our $TiAl_2$ preparation, D. S. Jones for the preparation of many of the alloys examined here, G. W. West for his substantial contribution to the design of the high-temperature probe, M. Forsyth for the loan of an MAS probe, and I. J. F. Poplett for obtaining the field sweep spectra. M.E.S. thanks the University of Kent for its support of solid-state NMR, and the EPSRC for access to the 14.1 T ultrahigh field facility.

[1] F. H. Froes, C. Suryanarayana, and D. Eliezer, J. Mater. Sci. **27**, 5113 (1992).
[2] A. Raman and K. Schubert, Z. Metallkd. **56**, 99 (1965).
[3] S. Mazdiyasni, D. B. Miracle, D. M. Dimiduk, M. D. Memdiratta, and P. R. Subramanian, Scr. Metall. **23**, 327 (1989).
[4] S. Zhang, J. P. Nic, and D. E. Mikkola, Scr. Metall. **23**, 1199 (1990).
[5] C. T. Forwood and M. A. Gibson, Mater. Sci. Forum **189-190**, 353 (1995).
[6] M. E. Smith, Appl. Magn. Reson. **4**, 1 (1993).
[7] L. E. Drain, Metall. Rev. **119**, 95 (1967).
[8] E. R. Andrew, Int. Rev. Phys. Chem. **1**, 191 (1981).
[9] T. J. Bastow and M. E. Smith, J. Phys.: Condens. Matter **7**, 4929 (1995).
[10] M. E. Smith, M. A. Gibson, C. T. Forwood, and T. J. Bastow, Philos. Mag. A **74**, 791 (1996).
[11] T. J. Bastow, M. E. Smith, and G. W. West, J. Phys.: Condens. Matter **9**, 6085 (1997).
[12] Y. M. Pan, S. T. Schwab, and P. P. Paul, Ceram. Trans. **54**, 151 (1995).
[13] *Pearson's Handbook of Crystallographic Data for Intermetallic Phases*, edited by P. Villars and L. D. Calvert (American Society for Metals, Metal Park, OH, 1985).
[14] A. C. Kunwar, G. L. Turner, and E. Oldfield, J. Magn. Reson. **69**, 124 (1986).
[15] T. J. Bastow, J. Phys.: Condens. Matter **8**, 11 309 (1996).
[16] R. V. Kasowski and L. M. Falicov, Phys. Rev. Lett. **22**, 1001 (1969), and references therein.
[17] E. F. W. Seymour, Proc. Phys. Soc. London, Sect. A **66**, 85 (1953).
[18] T. J. Bastow, M. A. Gibson, and C. T. Forwood, Solid State Nucl. Magn. Reson. (to be published).
[19] T. J. Bastow, M. E. Smith, and S. N. Stuart, Chem. Phys. Lett. **191**, 125 (1992).
[20] P. Blaha, K. Schwarz, and P. H. Dederichs, Phys. Rev. B **37**, 2792 (1988).
[21] M. Kogachi and A. Kameyama, Intermetallics **3**, 327 (1995).